PCCP

Prediction of optimal structural water concentration for maximized performance in tunnel manganese oxide electrodes

Journal:	*Physical Chemistry Chemical Physics*
Manuscript ID	CP-ART-02-2018-000761.R1
Article Type:	Paper
Date Submitted by the Author:	08-Mar-2018

Complete List of Authors:	Frey, Nathan; University of Pennsylvania, Materials Science and Engineering Byles, Bryan; Drexel University, Materials Science and Engineering Kumar, Hemant; University of Pennsylvania, Materials Science and Engineering Er, Dequan; University of Pennsylvania, Materials Science and Engineering Pomerantseva, Ekaterina; Drexel University, Materials Science and Engineering Shenoy, Vivek; University of Pennsylvania, Department of Materials Science and Engineering

Prediction of optimal structural water concentration for maximized performance in tunnel manganese oxide electrodes

Nathan C. Frey[†], Bryan W. Byles[‡], Hemant Kumar[†], Dequan Er[†], Ekaterina Pomerantseva*[,‡], and Vivek B. Shenoy*[,†]

[†]*Department of Materials Science and Engineering, University of Pennsylvania, Philadelphia, Pennsylvania 19104, USA*

[‡]*Department of Materials Science & Engineering, Drexel University, Philadelphia, Pennsylvania 19104, USA*

** Corresponding Authors, Email: vshenoy@seas.upenn.edu, ep423@drexel.edu*

Abstract

Crystal water has been shown to stabilize next-generation energy storage electrodes with structural tunnels to accommodate cation intercalation, but the stabilization mechanism is poorly understood. In this study, we present a simple physical model to explain the energetics of interactions between the electrode crystal lattice, structural water, and electrochemically cycled ions. Our model is applied to understand the effects of crystal water on sodium ion intercalation in a tunnel manganese oxide structure, and we predict that precisely controlling the crystal water concentration can optimize the ion intercalation voltage and capacity, and promote stable cycling. The analysis yields a critical structural water concentration by accounting for the interplay between elastic and electrostatic contributions to the free energy. Our predictions are validated with first-principles calculations and electrochemical measurements. The theoretical framework used here can be extended to predict critical concentrations of stabilizing molecules to optimize performance in next-generation battery materials.

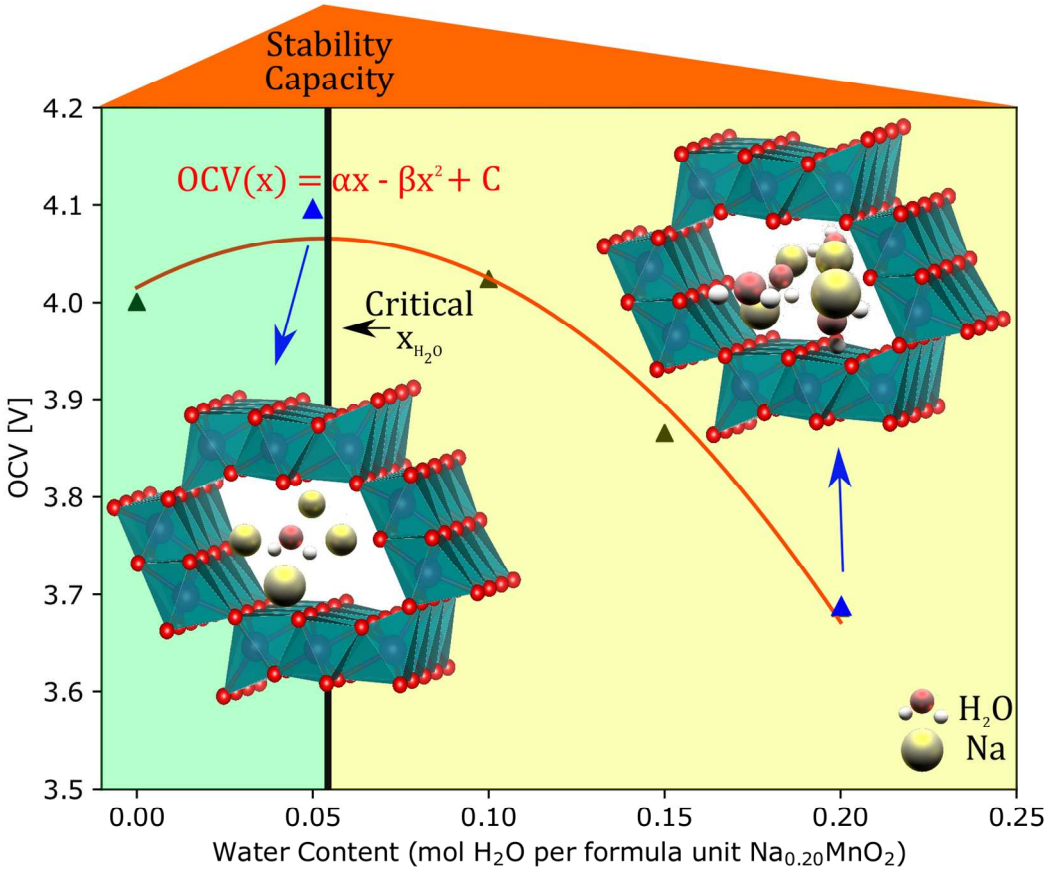
Stability
Capacity
OCV(x) = αx - βx² + C
Critical
x_H2O
OCV [V]
4.2
4.1
4.0
3.9
3.8
3.7
3.6
3.5
0.00
0.05
0.10
0.15
0.20
0.25
Water Content (mol H2O per formula unit Na0.20MnO2)
H2O
Na

Introduction

Growing energy demand and scarcity of lithium resources drives a need to transition from Li-ion batteries (LIBs) to cheaper, more sustainable alternatives. Na-ion batteries (NIBs) may be ideal for large scale energy storage applications where cost is especially important,[1–6] but this emerging technology is limited by currently available materials, including cathode materials. One promising family of NIB electrodes is manganese oxides with tunnel crystal structures.[7–9] Tunnel manganese oxides have shown reversible capacities of up to 128 mAh g^{-1} for Na^+ ions,[4] and are attractive because of their low cost and low toxicity.[10–13] However, repeated insertion/deinsertion of the relatively large, heavy Na^+ ions cause cycling capacity loss and shorter battery lifetimes in these tunnel oxide NIB materials.[4,7–9] To overcome these challenges, it is important to understand how a potential NIB electrode accommodates the size of the intercalating ion. The large open tunnels in tunnel manganese oxides, formed by MnO_6 octahedra, provide ample space for Na^+ ion insertion, but suitably large tunnels introduce structural instability in de-intercalated lattices.[6,14–17]

Tunnel manganese oxides with suitable crystallographic volume for ion intercalation contain both structural water molecules and stabilizing cations within their structural tunnels.[18] Tunnel manganese oxides are of particular interest because the size and shape of structural tunnels can be carefully tuned to optimize thermodynamic properties relevant for a battery electrode material, and the concentration of crystal water in tunnels can be controlled via post-synthesis annealing. Tailoring the synthesis conditions and stabilizing ion concentration allowed for experimental control of the tunnel volume, ensuring adequate space is available for high mobility ion intercalation. Stabilizing species occupy only a fraction of the sites within these tunnels, leaving sufficient empty volume for the insertion and diffusion of electrochemically

cycled ions. Recent theoretical and experimental studies have shown that structural water may play a part in facilitating large ion insertion and preventing deformation in layered crystal structures upon charge/discharge.[19–24] A possible explanation for this behavior is that crystal water forms a solvation shell and screens lattice-ion interactions to improve diffusion.[25–28] Due to inherent difficulties in decoupling the ion-lattice and ion-water interaction contributions to intercalation voltage, a fundamental physical understanding of the water-stabilization mechanism is still lacking. In this report, we seek to understand this mechanism and explain corresponding electrochemical observations.

Motivated by the promising performance of crystal water-containing tunnel manganese oxide structures in intercalation-based batteries, we propose a comprehensive physical model to elucidate the interplay of forces between the crystal lattice, structural water, and structural/electrochemically cycled ions. Our phenomenological model suggests a general framework for optimizing crystal water content in a broad class of next-generation electrode materials, which can be experimentally achieved through controlling post-synthesis annealing conditions for tunnel manganese oxides. This approach can be applied to address the critical challenge of maximizing stability for any tunnel structured transition-metal oxide electrode material, by predicting an ideal concentration of the stabilizing molecule. Here, we demonstrate the validity of our model by studying and characterizing a recently experimentally realized MnO_2 tunnel structure,[29] which we propose as a promising candidate for Na^+ ion cathode materials. This model system contains large structural tunnels for Na^+ ion diffusion and exhibits promising initial capacity in Na-ion cells,[30] as well as desirable intercalation voltages through precise control of crystal water concentration. We perform a thorough study of the intercalation compound based on density functional theory (DFT) simulations. In so doing, we predict an ideal

crystal water concentration and simultaneously address two key priorities in tunnel-oxide NIB electrodes: 1) maintaining stability during cycling despite the large, open structural tunnels, and 2) tuning ion binding energies to yield optimal intercalation voltages. Our model is validated by close agreement with both electrochemical measurements of the open circuit voltage (OCV) dependence on crystal water concentration and DFT simulation results.

Results

Crystal Structure Configurations

Before describing our model, we discuss the characterization of both the pristine 2x3-MnO_2 tunnel structure without stabilizing species and the structure stabilized by crystal water and Na^+ ions, and we demonstrate that this material is both a promising Na-ion cathode and a suitable model system for investigating the rich physics that govern the voltage window. The pristine crystal structure of the model 2x3-MnO_2 compound, without structural water and ions in the tunnels, is shown in Fig 1. Although 2x3-MnO_2 with tunnel structures cannot be synthesized without structural water and ions, we simulate both the pristine 2x3-MnO_2 system and the stabilized 2x3-$Na_{0.2}MnO_2$•0.20(H_2O) system to investigate the possible configurations of structural water and ions. As pictured in the supercell, each Mn atom is octahedrally coordinated by six oxygen atoms. The MnO_6 octahedra are arranged in a rectangular tunnel configuration, which accommodates a varying number of intercalating ions, as well as structural Na^+ ions and water molecules. The relaxed structure, pictured in Fig 1, has C2/m space group symmetry.

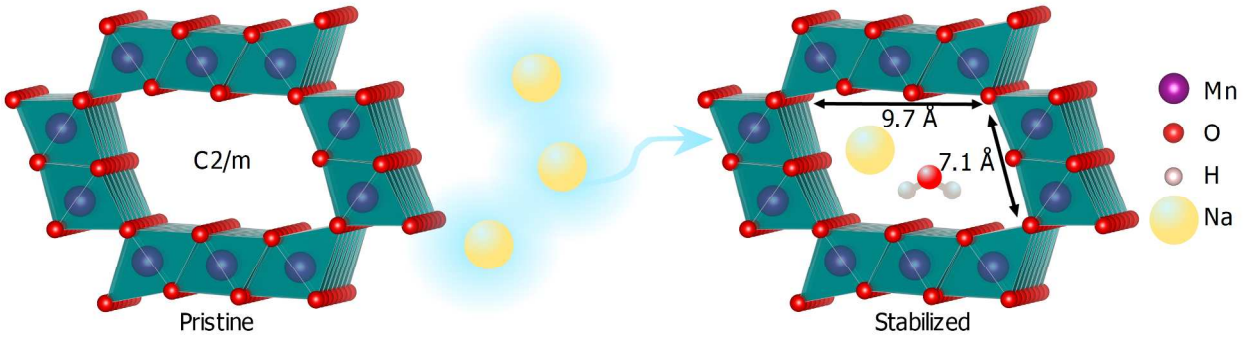

Fig 1. Schematic illustration of the pristine and stabilized 2x3-MnO_2 tunnel-oxide structures. Purple spheres are Mn atoms, red spheres are O atoms, white spheres are H atoms, and yellow spheres are Na atoms. The bare lattice after DFT relaxation has tunnel dimensions 7.1 Å x 9.7 Å, measured from Mn to Mn. The relaxed structure has space group symmetry C2/m. Experimentally, the most stable cathode configuration is found to be 2x3-$Na_{0.2}MnO_2$•0.20(H_2O), where a 0.2 concentration of crystal sodium and crystal water are found to stabilize the 2x3-MnO_2 lattice. Stabilizing species are shown within the tunnel, leaving sufficient crystallographic volume for electrochemically cycled Na^+ ions. Further, due to the relative amount of Na ions and water molecules present in the lattice, only a fraction of the unit cells in 2x3-MnO_2 are occupied by stabilizing species.

To understand the effects of structural water on sodium ion intercalation and provide insight into experimental observations, we investigate all possible combinations of H_2O molecules and Na+ ions residing in the tunnels of the 2x3-MnO_2 electrode. While the ground state lattice structure is known experimentally, we have determined the energetically favorable ion and water molecule adsorption sites within the tunnels by carrying out density functional theory simulations. DFT structure relaxations revealed an energy dependence on the orientation of water molecules. To fully explore the energy landscape of 2x3-MnO_2 with stabilizing water and ions, *ab initio* molecular dynamics (AIMD) simulations were used to probe the dynamics of crystal water reorientation and find the minimum energy orientations. As expected, the AIMD trajectories showed strong energetic favorability for water molecule orientations that maximize hydrogen-bond-like interactions between the stabilizing molecule, crystal lattice, and Na^+ ions. It should be noted there are three principle sites within each tunnel which a water molecule or

sodium ion may occupy. These sites lie along the diagonal plane between opposing octahedra on the long sides (three octahedron side) of the rectangular tunnels (Fig 1). We find that, beginning with a de-intercalated 2x3-MnO_2 crystal compound (no structural Na^+ ions or water molecules), possible intercalation pathways yield stable configurations for a unit cell with the following tunnel contents: one water molecule, two water molecules, one water molecule and one sodium ion, two sodium ions, or one water molecule and two sodium ions. Each of these states can be accommodated within the two by three octahedral tunnel without causing excessive volume expansion or lattice distortion that significantly breaks the symmetry of the unit cell and raises the binding energy. The optimal single unit cell configuration, in terms of capacity and per atom binding energy, as shown through calculations below, is two sodium ions separated by a crystal water molecule, as is shown in the right part of Figure 2. We first perform DFT simulations to calculate key electrode material properties and evaluate the 2x3-MnO_2 structure's viability as a NIB cathode. Of principle interest are the OCV, maximum theoretical capacity, and the volume change due to intercalation.

OCV and Ion-Water-Lattice Interactions

Ionic and electronic geometry relaxations yield a minimum energy configuration for the maximally intercalated structure (containing two Na^+ ions per $(MnO_2)_5$ unit cell, and no structural water), which is used as a benchmark to gauge the theoretically predicted performance of the 2x3-MnO_2 cathode. The insertion voltage is found to be 3.1 V, with a maximum theoretical capacity of 81.023 mAh g^{-1}. These results suggest that the 2x3-MnO_2 tunnel structure is a promising cathode material for Na^+ ion intercalation. We next turn to exploring the potential

of precisely controlled crystal water concentration to simultaneously increase energy density, cyclability, and insertion voltage.

Here, we present a general picture for the role of crystal water during intercalation. The potentials for no water and two Na^+ ions, one water and one Na^+ ion, and one water and two Na^+ ions are calculated to be 2.76 V, 4.17 V and 2.97 V vs Na/Na^+, respectively. An OCV increase of 0.21 V was found after adding water to the two ion structure, suggesting that fine-tuned improvements to insertion voltage can be made by understanding and leveraging the effects of stabilizing crystal water. Here, we decompose the interplay of forces between the manganese oxide lattice, intercalating charge-carrying ions, and crystal water. By decoupling the competing interactions, we were able to understand both the configuration of stabilizing Na^+ ions and water within the crystal tunnels, and the complete energetics that determine the insertion voltage and other thermodynamic properties of interest. We further examine the configuration with two Na^+ ions separated by one water molecule, as this is the most stable unit cell that includes all of the competing interactions of interest.

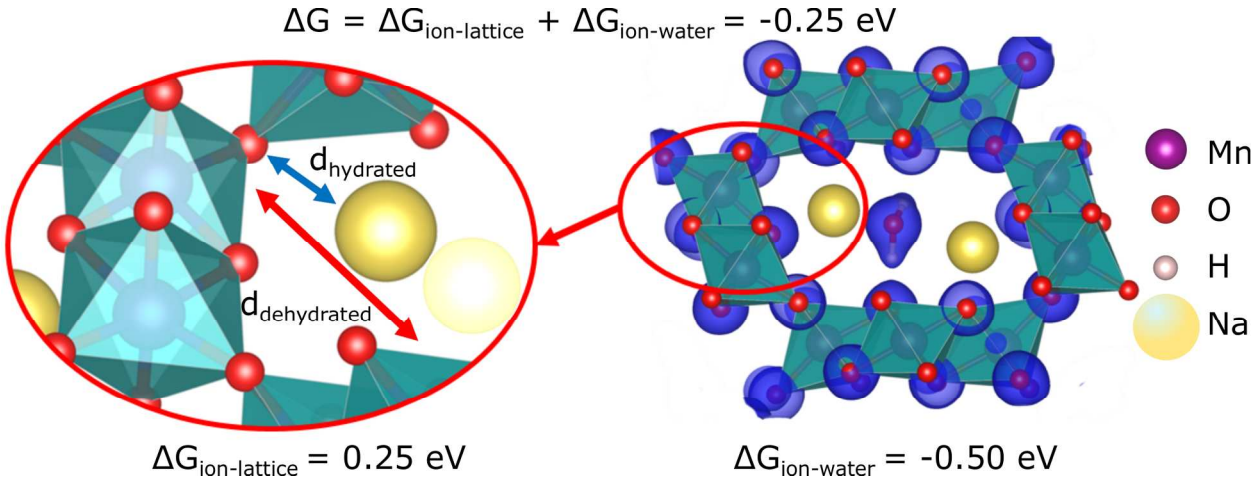

Fig 2. The charge density after hydration (right), where the Na-water interaction results in a -0.50 eV contribution to the Gibbs free energy. The red highlighted inset depicts the decrease in the distance between a Na^+ ion and the edge lattice oxygen, from 4.6 Å to 3.9 Å, after

hydration. Strain effects induce an energy penalty of 0.25 eV. The total change in the Gibbs free energy upon hydration is shown to be -0.25 eV.

The stabilizing effect of water is illustrated by energetics and Bader charge analysis shown in Fig 2. The lattice is fixed in the equilibrium geometry of the water + two Na^+ ion structure, to enable direct comparisons between the hydrated and dehydrated electronic structures. Computing the Bader charge density after hydration reveals the profound effect of water stabilization on the electronic environment within the tunnel structure. While the charge density on the lattice atoms remains relatively unchanged, after hydration there is an excess of electrons due to the introduction of water. This suggests complete charge transfer from the electrochemically inserted Na^+ ions to the lattice, regardless of the presence of crystal water. Therefore, we may expect that there is a strong electrostatic interaction between the dipolar water molecule and the positively charged ions. Next, we decouple the contributions to insertion voltage based on this electrostatic argument. The per-ion binding energies were computed for the dehydrated 2x3-MnO_2 structure with ion intercalation in the ground state geometry, as well as in the equilibrium geometry for the crystal structure with stabilizing water and electrochemically cycled ions. A difference of 0.25 eV was found, purely due to strain effects in the lattice in the hydrated ground state geometry. Therefore, we conclude that of the 0.25 V increase in the insertion voltage after hydration, a -0.25 V penalty is introduced by the ion-lattice interaction induced lattice strain (Fig 2, inset), while a 0.50 V increase results from a hydrogen-bonding-like interaction between the water molecule and cations (Fig 2, right).

Through Bader charge analysis, the Na^+ ions are found to be in their nominal +1 oxidation state after hydration and there is a partial negative charge of -0.6 e localized on the oxygen atom in the water molecule.[31] A simple electrostatic calculation using these partial

charges and the Na-water (Na-Na) distance of 2.5 Å (4.9 Å) gives a per-ion interaction energy of -517.2 meV, which is higher than a strong hydrogen bond, typically around -300 meV. This is to be expected due to the complete charge transfer of the Na valence electrons. Fig 3 shows the nature of this electrostatic interaction, and gives a simple analytic estimate of the attractive Coulombic contribution to the overall per-ion binding energy. The DFT calculated contribution to the binding energy due to the Na-water interaction is 0.50 eV, indicating that the simple calculation above is in good agreement with simulation. Taking into account all of these effects, our results explain the increase in binding energy within the lattice due to the presence of structural water.

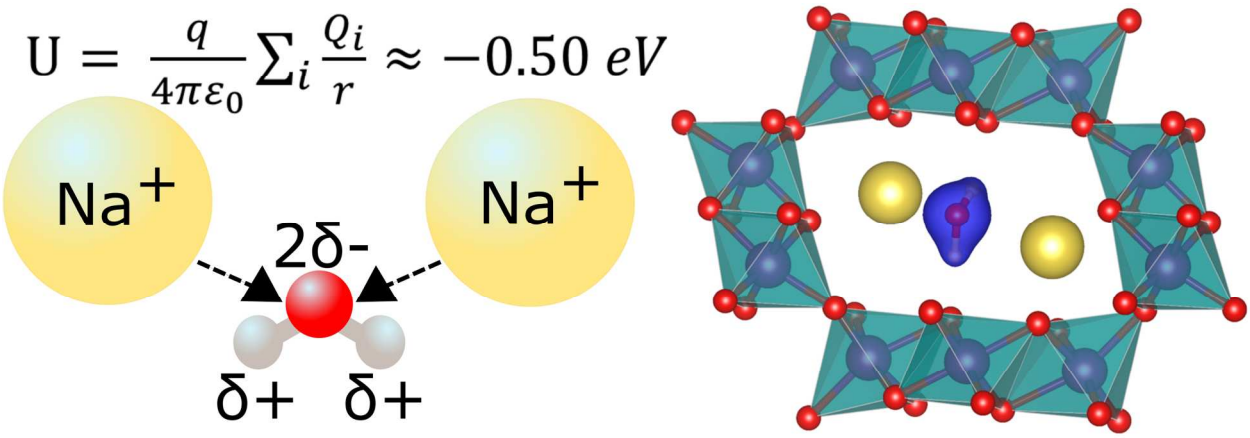

Fig 3. The electrostatic interaction (left) between positively charged Na^+ ions and dipolar water molecule. A simple analytical electrostatic calculation using atomic charges from Bader charge analysis and interatomic distances from DFT simulations yields an estimated binding energy on the order of -0.50 eV. The Bader charge density difference (right) before and after hydration shows complete charge transfer from Na to the 2x3-MnO_2 lattice, regardless of the presence of water.

Maximum Theoretical Capacity and Volume Change

A single unit cell was sufficient to elucidate the atomic-scale physics of the lattice-ion-water interactions and the resulting nanoscale structure and insertion voltage, but we next turn to the maximum theoretical capacity, which necessitates considering supercell configurations in the

x, *y* (in-plane) and *z* (out-of-plane) directions. Combinatorially, the number of possible equilibrium configurations increases dramatically when considering a 2x1x2 or 1x2x2 supercell, which can accommodate four discrete layers of any previously discussed water-ion arrangement. To reduce the number of possibilities to be considered, we first calculate ground state total energies and binding energies for supercells constructed in the in-plane directions. Unsurprisingly, electrostatic screening from the 2x3-MnO_2 lattice effectively decouples interactions between water-ion complexes in even nearest-neighbor tunnels. The ground state energies and insertion voltages for a single tunnel structure showed no dependence on the configuration of neighboring tunnels.

In the out-of-plane *z* direction along which tunnels are oriented, intercalating atoms may be stacked at regular intervals of a single MnO_6 octahedron *z*-dimension (3 Å from Mn to Mn). Here, there is minimal screening and it is expected that repulsive electrostatic ion-ion interactions may destabilize the structure and unfavorably impact maximum theoretical capacity, insertion voltage, and cyclability. Based on the findings for a single unit cell discussed above, the two sodium + one water configuration was considered optimal for a single layer. To explore a wide range of possible sodium concentrations and facilitate close comparison to experiment, capacities were calculated based on calculations of 1x1x2, 1x1x3, and 1x1x4 supercells, with up to 76 atoms in a supercell. At a structural water concentration $x_{H_2O} = 0.2$, we predict a maximum theoretical capacity of 51 mAh g^{-1}, corresponding to an increase in Na concentration from $x_{Na} = 0.2$ (purely structural Na^+ ions) to $x_{Na} = 0.40$, after electrochemical cycling. The capacity calculations are detailed later in the discussion and compared directly to electrochemical measurements.

General trends emerge based on the results of the volumetric and ionic relaxations. Intercalation of large sodium ions caused dramatic tunnel volume expansion, while hydration resulted in a more minimal expansion. Between the unit cell with structural Na^+ ions, corresponding to $x_{Na} = 0.2$, and the maximally intercalated unit cell ($x_{Na} = 0.4$) there is a 3.4% volume increase, from 189.9 $Å^3$ to 196.4 $Å^3$, without structural water. With structural water, the volume change due to intercalation is 1.7%, from 199.2 $Å^3$ to 202.6 $Å^3$. Coexistence of water and sodium, rather than causing additive volume expansion, was found to reduce the effects of expansion due to pure sodium intercalation. The presence of a coordinating water molecule between two intercalating sodium ions clearly reduces volume expansion compared to dehydrated intercalation, and therefore may be expected to improve cycling stability.

Analytic Model

Based on the predictions above and the success in decoupling the ion-ion, ion-water, and ion-lattice interactions, we propose an intuitive and universal physical description of the role of crystal water in electrode materials. As shown above, the per-ion binding energy is dependent on the strain induced by the coexistence of stabilizing molecules and ions, as well as the favorable electrostatic interaction between crystal water and Na^+ ions. Because of the total charge transfer from Na^+ ions to the 2x3-MnO_2 lattice, regardless of hydration, the ion-lattice interaction is expected to be approximately constant for constant sodium concentration, x_{Na}. The electrostatic contribution should be nearly linearly dependent on water concentration, while strain energy goes as ϵ^2 or σ^2, where ϵ is strain and σ is stress. Therefore, the contribution from strain is quadratic in the water concentration. The free energy, then, can be modelled analytically as

$$G(x) \sim -\alpha x + \beta x^2$$

where x is the water concentration, and α and β are coefficients that depend on the sodium concentration. In this phenomenological model, higher order terms of $O(x^3)$ in the water concentration can be neglected in the dilute limit $\frac{x_{H_2O}}{x_{MnO_2}} \ll 1$.

With this picture in mind, we predict that at a given sodium concentration x_{Na}, the measured OCV profile of $Na_{x_{Na}}MnO_2$ as a function of water concentration will have an approximately quadratic form in which OCV increases with increasing water concentration in the range $x \epsilon [0, \frac{\alpha}{2\beta}]$, and OCV decreases with increasing water concentration for $x > \frac{\alpha}{2\beta}$. Consequently, the measured OCV is predicted to be the same at $x = 0$ and $x = \frac{\alpha}{\beta}$, the critical water concentration at which the strain and electrostatic contributions perfectly cancel out.

Experimental and Predicted OCV as a Function of Water Concentration

In order to test our theoretical predictions and validate the above model, we perform electrochemical experiments using working electrodes of 2xn-MnO_2. A description and experimental characterization of this material can be found in supporting information, Figure S1. The water content of this material is controlled through annealing at different temperatures prior to electrochemical experiments, and the water content of the 2xn-$Na_{0.20}MnO_2$ was calculated from thermogravimetric analysis (TGA) data (Figure S1). Indeed, both experimental measurements and DFT simulations for $Na_{0.20}MnO_2 \cdot 0.18(H_2O)$ confirm that this simple model is correct. Fig 4 depicts experimental (Fig 4, top) and theoretical (Fig 4, bottom) OCVs as a function of water concentration. The trend predicted by our model is seen exactly in both plots, and we fit the DFT results to obtain the coefficients α and β, which are 2.1659 eV/mol and 19.097 eV/mol^2, respectively. Based on these values we predict a critical water concentration,

$x_{crit} = 0.0567$, which delineates the electrostatic dominated (Fig 4, green shaded region) and strain dominated (Fig 4, yellow shaded region) regions of the OCV profile. This prediction agrees with the experimental characterization of the OCV profile of the 2xn-$Na_{0.20}MnO_2 \bullet n(H_2O)$ (n=0.05-0.18) electrodes.

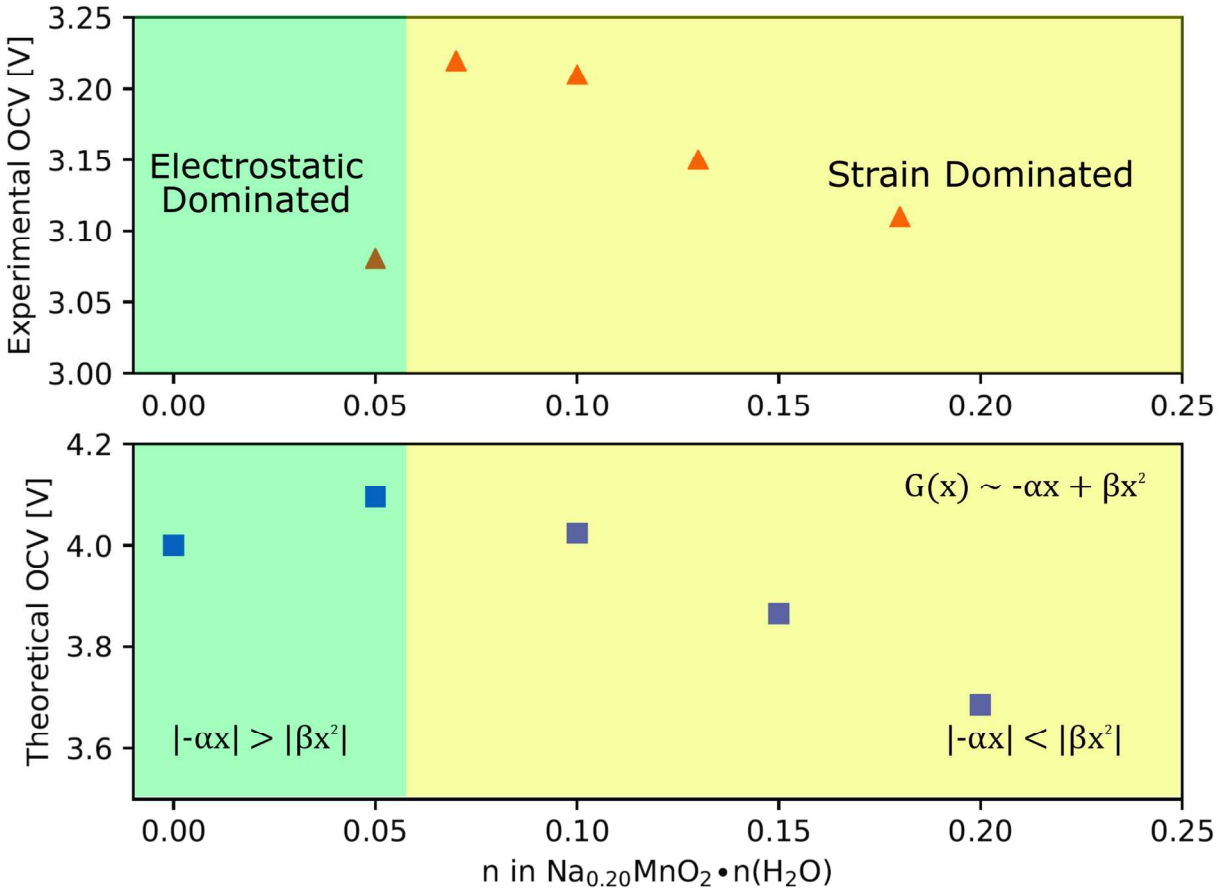

Fig 4. Experimental (top) and theoretical (bottom) open circuit voltage in Na-ion cells of $Na_{0.20}MnO_2$ as a function of water content. The trend predicted by the simple free energy model $G(x) \sim -\alpha x + \beta x^2$ is observed both in DFT calculations and experiment. At low water content (green shaded region), the favorable electrostatic ion-water interaction dominates, while at high water content (yellow shaded region), the unfavorable strain contribution dominates.

Because there are no system-specific assumptions made in this model, we expect that our results provide a generalized framework that can be applied to any nanostructured intercalation material stabilized with structural water. In particular, our model can be used to optimize the water:ion concentration ratio to yield favorable insertion voltages and maximally efficient cycling. Here, the crystal structure is stable at each water concentration, and the water content is controlled experimentally through annealing. Thus, the water content can be optimized by annealing at appropriate temperatures – meaning that there is no risk of structural water being ejected to the electrolyte during charge and discharge cycles.[19]

Experimental and Theoretical Capacity

Table 1 summarizes the experimental values for capacity measured in the first and second charge and discharge cycles. Most notably, there is a significant increase in capacity after the first discharge. Theoretical predictions of the capacities agree well with experiment, indicating that the configurations shown in Fig 5 represent the equilibrium charged and discharged states.

	Capacity [mAh g^{-1}]			
Cycle	Measured Discharge	Theoretical Discharge	Measured Charge	Theoretical Charge
1st	48	51	63	63
2nd	60	63	59	63

Table 1. Measured and theoretical discharge and charge capacities [mAh g^{-1}] on 1st and 2nd cycles.

Fig 5 shows top-down views of a single 2x3-MnO_2 tunnel from a 1x1x4 supercell, with the top-most layer of MnO_6 octahedra removed so that the sodium and water configurations can be easily seen. Fig 5a is the stabilized charged state, with stoichiometry $Na_{0.20}MnO_2(H_2O)_{0.20}$. Upon first discharging, sodium ions are intercalated into the cathode (Fig 5b) and the new sodium concentration is $x_1 = 0.40$, that is, the sodium concentration doubles during the first

discharge. The experimentally measured first discharge capacity of 48 mAh g^{-1} agrees well a predicted value of 51.2 mAh g^{-1} (Table 1, Figure 5a). On the subsequent discharge (Fig 5b), a higher sodium concentration of $x_2 = 0.45$ gives an increased capacity of 63.3 mAh g^{-1}, which also agrees remarkably well with the experimentally observed capacity of 63 mAh g^{-1}.

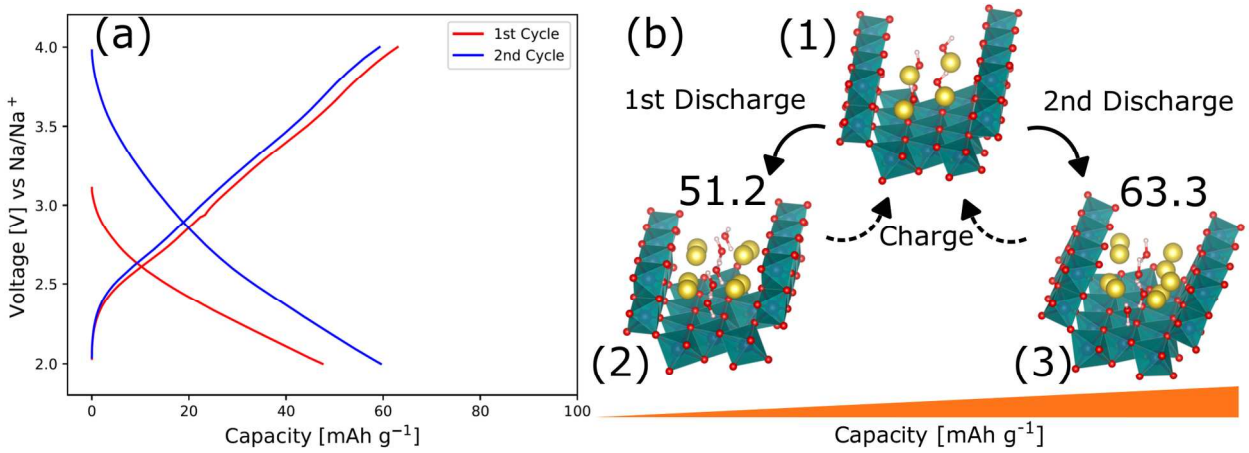

Fig 5. First (red) and second (blue) discharge-charge cycles (a) of the 2xn-MnO_2 under galvanostatic conditions (C/10 rate). The theoretical value (b) for the capacity on first discharge from the ground state (1) to the intercalated state (2) is 51.2 mAh g^{-1}. A higher capacity of 63.3 mAh g^{-1} is predicted for subsequent cycles between the ground state and the highly sodiated discharged state (3). These values agree to within mAh g^{-1} with experiment.

To understand why the second pathway is not taken during the first discharge, we again consider the competing strain and ion-water interactions. By repeating the calculations detailed above, for the 1x1x4 $Na_{0.20}MnO_2 \bullet 0.20(H_2O)$ supercell, we find that the purely structural sodium concentration results in a negligible -0.04 eV attractive ion-water interaction; the state shown in Fig 5a is firmly in the strain dominated region of the OCV(x) profile. Intercalating increasing numbers of Na^+ ions becomes increasingly favorable, as the higher concentration of

sodium results in a larger attractive Coulombic interaction. However, to accommodate the doubling sodium concentration, the 2x3-MnO_2 unit cell expands from 183 $Å^3$ to 195 $Å^3$, a 6% increase. During the first discharge, the lattice expands and the crystal water molecules reorganize, allowing for increased sodium-ion intercalation on subsequent discharges. In the highest observed capacity configuration, the per unit cell volume is 197 $Å^3$, which is a minor 1% increase compared to the volume corresponding to the $x_1 = 0.40$ state. An additional mechanism involving the extraction of stabilizing Na^+ ions upon discharge, such that the charged state has $x_{Na} < 0.20$, can also explain the measured capacities, but this picture is discarded as energy dispersive X-ray spectroscopy (EDX) measurements on electrodes before and after first discharge and charge cycles indicate that the sodium concentration for the stabilized lattice is never significantly reduced beyond 0.20 (see Supplementary Table 1).

In conclusion, we have proposed a general phenomenological model to explain the interplay of interactions between transition-metal oxide lattices, stabilizing species (Na^+ ions and water molecules), and electrochemically cycled ions. Using our model to decouple these interactions, we were able to predict an optimal structural water concentration to minimize volume expansion, and optimize intercalation voltage and capacity of a model tunnel manganese-oxide NIB cathode. We found that by tuning the structural water concentration according to our model predictions, desirable battery performance metrics can be precisely controlled. Our predictions were validated through close agreement with electrochemical experiments and DFT simulations. It is expected that the method developed here will be applicable to other tunnel manganese oxide phases of interest for energy storage that contain structural water in their tunnels, including α-MnO_2, Todorokite MnO_2, and Na-2x4.[32] The general physical picture presented in this study will be helpful not only in optimizing

performance of next-generation battery materials, but also in moving beyond crystal water to find other molecules that can stabilize new NIB electrodes, improve cycling stability, and tune intercalation voltages.

Methods

Our DFT calculations were performed with the Vienna Ab-Initio Simulation Package (VASP).[33] Projector augmented wave (PAW) pseudopotentials[34] were used with an energy cutoff of 520 eV for plane-wave expansions. The Perdew-Burke-Ernzerhof (PBE) generalized gradient approximation (GGA) to the exchange-correlation functional was used.[35] To account for the strongly-correlated Mn transition metal in the intercalation compound, all electronic structure calculations and geometry relaxations were done with the spin polarized DFT+U correction.[36,37] A U value of 4 eV was used for Mn, as is typical in the literature, for the on-site Coulombic repulsion. A Γ-centered k-point mesh of 6 x 6 x 6 in the first Brillouin zone yielded well-converged results for structural relaxations of the unit cell. The Γ-centered k-point mesh was reduced to 3 x 2 x 3 for supercell volume relaxations and 4 x 4 x 4 for supercell ionic relaxations. Atomic positions within unit cells and supercells were optimized to within 0.01 eV/ Å force on each atom. Total energy changes were converged to within 10^{-6} eV. Near-dilute and high concentrations of Na ions were simulated by considering 1 x 4 x 1 supercells, extended along the tunnel direction, to accommodate varying numbers of Na ions per tunnel.

OCVs were obtained in the usual way, by considering the intercalation reaction

$$\mathrm{MnO_2} + x\mathrm{Na} \rightarrow \mathrm{Na}_x\mathrm{MnO_2} \#(1)$$

where x is the number of Na intercalated into the lattice per formula unit of 2x3-MnO_2.[36,38] The change in Gibbs free energy, ΔG, is calculated by making the following approximation and neglecting pressure and entropy contributions to the enthalpy,

$$\Delta G = \Delta E + p\Delta V - T\Delta S \approx \Delta E \#(2)$$

which is commonly made, as $T\Delta S$ is nearly 25 meV at room temperature, and $p\Delta V$ is also negligible compared to ΔE.[36,38] The formation energy associated with the intercalation process is then defined as

$$\Delta E = \frac{E_{\mathrm{Na}_{x_2}\mathrm{MnO}_2} - \left((x_2 - x_1)\mu_{\mathrm{Na}} + E_{Na_{x_1}\mathrm{MnO}_2}\right)}{x_2 - x_1} \#(3)$$

where μ_{Na} is the chemical potential of Na in the bulk BCC phase, $E_{\mathrm{MnO_2Na}_x}$ is the ground state energy of the system after intercalation, and E_{MnO_2} is the ground state energy of the bare 2x3-MnO_2 lattice. Finally, the insertion voltage is defined in terms of the change in Gibbs free energy with a reference state $x_{Na} = 0$ (Equation 4), or a reference state $x_{Na} \neq 0$ (Equation 5) as

$$OCV = -\frac{\Delta G}{x} \approx -\frac{\Delta E}{x} \#(4)$$

$$OCV = -\mu = -\frac{\delta G}{\delta x} \approx -\frac{\Delta E}{\Delta x} \#(5)$$

Due to the energy dependence on the position and orientation of structural water molecules, *ab initio* molecular dynamics (MD) with a Nosé-Hoover constant-temperature (canonical ensemble) thermostat, as implemented in VASP,[33] was used to generate many possible configurations of water molecules in 1 x 4 x 1 supercells. Because exact energies were not required, and MD simulations are computer-intensive for large supercells,[39] the energy cutoff for plane-wave expansions was reduced to 280 eV and only the Γ point was sampled in the Brillouin zone. The time-step for each MD step was taken to be 1 femtosecond, with each simulation proceeding for 256 steps.

X-ray powder diffraction patterns of the 2xn-MnO_2 nanowires were recorded using a Rigaku SmartLab X-Ray Diffractometer (Japan) with Cu-Kα radiation source. Scanning

electron microscopy (SEM) images were obtained using a Zeiss Supra 50VP (Germany) SEM with an energy dispersive X-ray spectroscopy (EDS) attachment. Na:Mn ratios in electrodes of 2xn-MnO_2 nanowires were calculated from quantification of three EDS spectra recorded in separate 10 micron by 10 micron areas.

In order to systematically remove water from the 2xn-MnO_2 nanowires, the materials were annealed in air for four hours at various temperatures ranging from 100-400° C. Thermal gravimetric analysis (TGA) of the 2xn-MnO_2 nanowires was performed using a TA Instruments Q50 TGA under air environment from room temperature up to 800° C at a heating rate of 10° C min^{-1}.

Electrodes of 2xn-MnO_2 nanowires were prepared by mixing the active material, conductive additive (acetylene black, Alfa Aesar), and polymer binder (poly(vinylidene fluoride), Kynar) in a 7:2:1 ratio, respectively, in 1-methyl-2-pyrrolidinone (Alfa Aesar). The resulting slurry was casted onto an Al-foil current collector (Fisher Scientific) using a doctor blade method, and the electrode films were dried for 12 hours at room temperature followed by 1 hour at 100° C in air. After drying, individual electrode discs of 12 mm in diameter were punched and dried at 100° C under vacuum for 12 hours before transferring into an Ar-filled glovebox (H_2O < 0.5 ppm, O_2 < 0.5 ppm; MBRAUN). Na-ion batteries were assembled in the glovebox using two-electrode coin cells (2032 type) in half-cell configurations. The working electrode was the 2xn-MnO_2 nanowires, and the counter and reference electrodes were sodium metal (Sigma Aldrich). 1M $NaClO_4$ (Sigma Aldrich) in propylene carbonate and ethylene carbonate in a 1:1 ratio with a 5 vol. % fluoroethylene carbonate additive (BASF Chemicals) was used as the electrolyte, and glass microfiber filter (Whatman) was utilized as the separator. Cells were allowed to rest under ambient conditions for 2 hours before OCV measurements were made

on a battery testing station (Arbin Instruments). In order to evaluate the Na:Mn ratio in cycled electrodes, coin cells containing the cycled electrodes were disassembled in the glovebox, and the working electrodes were removed and thoroughly washed with propylene carbonate to remove any residual electrolyte.

Acknowledgments:

The authors acknowledge funding from the National Science Foundation under Grant CBET-1604483 for materials synthesis and electrochemical testing. N.C.F. was supported by the Department of Defense (DoD) through the National Defense Science & Engineering Graduate Fellowship (NDSEG) Program.

Supporting Information. Details of synthesis procedure and characterization of 2xn-MnO_2. SEM images, EDX spectrum, XRD pattern of nanowires, cross-section STEM, TGA, and Na:Mn ratio from EDX measurements of electrodes before cycling, after first discharge, and after one discharge + charge cycle.

References

1. Han, M. H., Gonzalo, E., Singh, G. & Rojo, T. A comprehensive review of sodium layered oxides: powerful cathodes for Na-ion batteries. *Energy Environ. Sci.* **8,** 81–102 (2015).
2. Kim, S.-W., Seo, D.-H., Ma, X., Ceder, G. & Kang, K. Electrode Materials for Rechargeable Sodium-Ion Batteries: Potential Alternatives to Current Lithium-Ion Batteries. *Adv. Energy Mater.* **2,** 710–721 (2012).
3. Kundu, D., Talaie, E., Duffort, V. & Nazar, L. F. The Emerging Chemistry of Sodium Ion Batteries for Electrochemical Energy Storage. *Angew. Chemie Int. Ed.* **54,** 3431–3448 (2015).
4. Slater, M. D., Kim, D., Lee, E. & Johnson, C. S. Sodium-Ion Batteries. *Adv. Funct. Mater.* **23,** 947–958 (2013).
5. Yabuuchi, N., Kubota, K., Dahbi, M. & Komaba, S. Research Development on Sodium-Ion Batteries. (2014). doi:10.1021/CR500192F
6. Verónica Palomares *et al.* Na-ion batteries, recent advances and present challenges to become low cost energy storage systems. *Energy Environ. Sci.* **5,** 5884–5901 (2012).
7. Devaraj, S. & Munichandraiah, N. Effect of crystallographic structure of MnO2 on its electrochemical capacitance properties. *J. Phys. Chem. C* **112,** 4406–4417 (2008).
8. Dawei Su, Hyo-Jun Ahn & Guoxiu Wang. Hydrothermal synthesis of α-MnO 2 and β-MnO 2 nanorods as high capacity cathode materials for sodium ion batteries. *J. Mater. Chem. A* **1,** 4845–4850 (2013).
9. Liu, Q. *et al.* Multiangular Rod-Shaped Na $_{0.44}$ MnO $_2$ as Cathode Materials with High Rate and

Long Life for Sodium-Ion Batteries. *ACS Appl. Mater. Interfaces* **9,** 3644–3652 (2017).

10. Tarascon, J. M. The Spinel Phase of LiMn2O4 as a Cathode in Secondary Lithium Cells. *J. Electrochem. Soc.* **138,** 2859 (1991).

11. Armstrong, A. R. & Bruce, P. G. Synthesis of layered LiMnO2 as an electrode for rechargeable lithium batteries. *Nature* **381,** 499–500 (1996).

12. Thackeray, M. M. & Engineering, C. Manganese oxides for lithium batteries. *Prog. Solid State Chem.* **25,** 1–71 (1997).

13. Chabre, Y. & Pannetier, J. Structural and electrochemical properties of the proton / γ-MnO2 system. *Progress in Solid State Chemistry* **23,** 1–130 (1995).

14. Doeff, M. M., Richardson, T. J. & Kepley, L. Lithium Insertion Processes of Orthorhombic Na x MnO2□Based Electrode Materials. *J. Electrochem. Soc.* **143,** 2507–2516 (1996).

15. F. Sauvage, L. Laffont, J.-M. Tarascon, and & Baudrin*, E. Study of the Insertion/Deinsertion Mechanism of Sodium into Na0.44MnO2. (2007). doi:10.1021/IC0700250

16. Tevar, A. D. & Whitacre, J. F. Relating Synthesis Conditions and Electrochemical Performance for the Sodium Intercalation Compound Na4Mn9O18 in Aqueous Electrolyte. *J. Electrochem. Soc.* **157,** A870–A875 (2010).

17. Cao, Y. *et al.* Reversible sodium ion insertion in single crystalline manganese oxide nanowires with long cycle life. *Adv. Mater.* **23,** 3155–3160 (2011).

18. Post, J. E., Heaney, P. J. & Hanson, J. Synchrotron X-ray diffraction study of the structure and dehydration behavior of todorokite. *Am. Mineral.* **88,** 142–150 (2003).

19. Nam, K. W. *et al.* The High Performance of Crystal Water Containing Manganese Birnessite Cathodes for Magnesium Batteries. *Nano Lett.* **15,** 4071–4079 (2015).

20. Nam, K. W. *et al.* Critical Role of Crystal Water for a Layered Cathode Material in Sodium Ion Batteries. *Chem. Mater.* **27,** 3721–3725 (2015).

21. Sai Gautam, G., Canepa, P., Richards, W. D., Malik, R. & Ceder, G. Role of Structural H2O in Intercalation Electrodes: The Case of Mg in Nanocrystalline Xerogel-V2O5. *Nano Lett.* acs.nanolett.5b05273 (2016). doi:10.1021/acs.nanolett.5b05273

22. Qiulong Wei *et al.* Hydrated vanadium pentoxide with superior sodium storage capacity. *J. Mater. Chem. A* **3,** 8070–8075 (2015).

23. Yang, Z. *et al.* Probing the Release and Uptake of Water in α□MnO 2 ·xH 2 O. doi:10.1021/acs.chemmater.6b03721

24. Zhu, K. *et al.* Tunable Electrochemistry via Controlling Lattice Water in Layered Oxides of Sodium-Ion Batteries. *ACS Appl. Mater. Interfaces* **9,** 34909–34914 (2017).

25. Novák, P. & Desilvestro, J. Electrochemical Insertion of Magnesium in Metal Oxides and Sulfides from Aprotic Electrolytes. *J. Electrochem. Soc.* **140,** 140 (1993).

26. Levi, E., YGofer & Aurbach, D. On the way to rechargeable Mg batteries: The challenge of new cathode materials. *Chem. Mater.* **22,** 860–868 (2010).

27. Kim, H. *et al.* Sodium intercalation chemistry in graphite. *Energy Environ. Sci.* **8,** 2963–2969 (2015).

28. Lim, S. Y. *et al.* Lattice Water for the Enhanced Performance of Amorphous Iron Phosphate in Sodium-Ion Batteries. *ACS Energy Lett.* **2,** 998–1004 (2017).

29. Byles, B. W., Cullen, D. A., More, K. L. & Pomerantseva, E. Tunnel structured manganese oxide nanowires as redox active electrodes for hybrid capacitive deionization. *Nano Energy* (2017). doi:10.1016/j.nanoen.2017.12.015

30. Li, J.-Y. *et al.* Romanechite-structured $Na_{0.31}MnO_{1.9}$ nanofibers as high-performance cathode material for a sodium-ion battery. *Chem. Commun.* **51,** 14848–14851 (2015).

31. Clites, M. & Pomerantseva, E. Bilayered vanadium oxides by chemical pre-intercalation of alkali and alkali-earth ions as battery electrodes. *Energy Storage Mater.* **11,** 30–37 (2018).

32. Suib, S. L. Structure, porosity, and redox in porous manganese oxide octahedral layer and molecular sieve materials. *J. Mater. Chem.* **18,** 1623 (2008).

33. Kresse, G. & Furthmüller, J. Efficient iterative schemes for ab initio total-energy calculations using a plane-wave basis set. *Phys. Rev. B* **54,** 11169–11186 (1996).

34. Kresse, G. & Joubert, D. From ultrasoft pseudopotentials to the projector augmented-wave method. *Phys. Rev. B* **59,** 1758–1775 (1999).

35. Perdew, J. P., Burke, K. & Ernzerhof, M. Generalized Gradient Approximation Made Simple. *Phys. Rev. Lett.* **77,** 3865–3868 (1996).

36. Zhou, F., Cococcioni, M., Marianetti, C. A., Morgan, D. & Ceder, G. First-principles prediction of redox potentials in transition-metal compounds with LDA + U. *Phys. Rev. B* **70,** 235121 (2004).

37. Jain, A. *et al.* Formation enthalpies by mixing GGA and GGA + U calculations. *Phys. Rev. B - Condens. Matter Mater. Phys.* **84,** 45115 (2011).

38. Aydinol, M. K., Kohan, A. F. & Ceder, G. Ab initio calculation of the intercalation voltage of lithium-transition-metal oxide electrodes for rechargeable batteries. *J. Power Sources* **68,** 664–668 (1997).

39. Zhao, X., Ceresoli, D. & Vanderbilt, D. Structural, electronic, and dielectric properties of amorphous Zr O 2 from *ab initio* molecular dynamics. *Phys. Rev. B* **71,** 85107 (2005).